Journal of Alloys and Compounds 509 (2011) 8798–8803

Contents lists available at ScienceDirect

Journal of Alloys and Compounds

journal homepage: www.elsevier.com/locate/jallcom

Synthesis and characterization of mesoporous Mn-MCM-41 materials

Maria Luisa Saladino[a,*], Elka Kraleva[b], Silvia Todorova[b], Alberto Spinella[c], Giorgio Nasillo[c], Eugenio Caponetti[a,c]

[a] Dipartimento di Chimica Fisica "S. Cannizzaro" and INSTM UdR Palermo, Università di Palermo, Parco d'Orleans II, Viale delle Scienze pad.17, Palermo 90128, Italy
[b] Institute of Catalysis, Bulgarian Academy of Sciences, 1113 Sofia, Bulgaria
[c] Centro Grandi Apparecchiature-UniNetLab, Università di Palermo, Via Marini 14, Palermo 90128, Italy

ARTICLE INFO

Article history:
Received 30 November 2010
Received in revised form 15 June 2011
Accepted 16 June 2011
Available online 23 June 2011

Keywords:
Composite materials
Surfaces
^{29}Si {^{1}H} CP-MAS NMR
X-ray photo-emission spectroscopy

ABSTRACT

MCM-41 has been synthesized at two different pH using cetyl-trimethylammonium bromide (CTAB) surfactant as template and adding the silica precursor to aqueous solutions containing CTAB. The obtained solids were calcined at 600 °C for 4 h. Mn-MCM-41 powders with different Mn/Si molar ratios were prepared using the incipient wetness method, followed by calcination at 550 °C for 5 h. At the end of the impregnation process the powders colour changed from white to brown whose intensity depends on manganese quantity. The materials characterization was performed by X-ray diffraction, N_2 adsorption, ^{29}Si Cross Polarization–Magic Angle Spinning NMR, and X-ray Photoelectron Spectroscopy. The effects of the manganese quantity and of the structural characteristic of the MCM-41 support were studied. The catalytic activity of the prepared systems was evaluated in a complete *n*-hexane oxidation.

1. Introduction

Recently, much attention has been paid to MCM-41 silicate molecular sieve with unidimensional mesopores [1–3]. It possesses a high surface area (>1000 $m^2\ g^{-1}$), a large pore volume, and a uniform pore size distribution in the mesoporous range. However, its framework is amorphous silica and contains a considerable amount of silanol groups. The incorporation of transition metal ions into micro- or mesoporous molecular sieves is of great interest for catalytic applications. In the last years, many metals were incorporated into the MCM-41 framework and the properties of the material were improved [4–7]. MCM-41 functionalisation with manganese leads to an active heterogeneous catalyst for various oxidation reactions [8,9]. Manganese is an environmentally friendly active component for many catalyst systems [10]. Its catalytic properties are attributed to its ability to change its oxidation states. A catalyst constituted by MCM-41 and manganese can combine the single properties of the two components increasing the catalytic performance. It has been reported that manganese can be incorporated into mesoporous molecular sieves [11]. Parida et al. prepared a catalyst for a single-step amination of benzene to aniline doping the MCM-41 with Mn(II) [12]. Some authors anchored a complex containing Mn atoms on the MCM-41 internal walls [13]. Other authors prepared a catalyst constituted by manganese oxides supported on silica [14].

The scope of this work is to study the influence of synthesis parameter such as pH and quantity of manganese, on the Mn-MCM-41 material. The synthesis of manganese oxide supported on the MCM-41 was performed using the incipient wetness method. A detailed characterization of the materials was made using X-ray Diffraction (XRD), N_2 adsorption–desorption isotherms, ^{29}Si Cross Polarization–Magic Angle Spinning NMR (^{29}Si {^{1}H} CP–MAS NMR), and X-ray Photoelectron Spectroscopy (XPS). The catalytic activity was evaluated in a complete *n*-hexane oxidation [14]. Hexane has been chosen because it is a component of many industrial products. In the air it participates in a radical reaction yielding 2-hexanone, 2-and 3-hexyl nitrate and 5-hydroxy-2-pentanone, all of them existing in the photochemical smog.

2. Experimental

2.1. Materials

Cetyltrimetylammonium bromide (CTAB, Aldrich), manganese nitrate tetrahydrate (Aldrich), hydrochloric acid (Aldrich, 37%), ammonia solution (Aldrich, 28%) ethanol (Fluka), tetraethoxysilane (TEOS, Fluka), *n*-hexane (Fluka) were used as received. Solutions were prepared by weight adding conductivity grade water.

2.2. Samples preparation

MCM-41: Two samples were prepared at different pH. The sample A was prepared at pH equal to 1. CTAB, hydrochloric acid, water and TEOS were mixed together as reported in our previous work [15]. The resulting gel was stirred for two hours. The sample B was prepared at pH equal to 8. CTAB, ethanol, ammonia and water were mixed together and the mixture was stirred for 45 min. Then, the silica precursor, TEOS, was added to the basic aqueous solution. The components of the mixture were in the following molar ratios: $CTAB/SiO_2 = 0.6$, $NH_4OH/SiO_2 = 12.5$, $EtOH/SiO_2 = 12$ and $H_2O/SiO_2 = 174$. The resulting gel was stirred for 2 h.

* Corresponding author. Tel.: +39 091 6459842; fax: +39 091 590015.
E-mail address: saladinoluisa@unipa.it (M.L. Saladino).

0925-8388/$ – see front matter © 2011 Elsevier B.V. All rights reserved.
doi:10.1016/j.jallcom.2011.06.078

The two obtained precipitates were recovered by filtration after 24 h, washed, dried at room temperature and calcined on air at 600 °C for 4 h.

Mn-MCM-41: Two different aliquots of sample ***A*** were used to prepare samples with Mn/Si atomic ratio (R) equal to 0.012 and 0.05. Two different aliquots of sample B were used to prepare samples with Mn/Si atomic ratio (R) equal to 0.006 and 0.025. Calcined mesoporous silica samples were treated with ethanol solutions containing the adequate quantity of manganese nitrate, following the incipient wetness method [16]. Samples were treated for 24 h at 60 °C to remove the ethanol. The dry materials were thermal treated at 550 °C for 5 h. The white MCM-41 powder became brown after impregnation. Two aliquots of non-impregnated A and B samples were treated at the same conditions to be used as reference samples (called A' and B').

2.3. Characterization methods

Powder X-ray Diffraction (XRD) patterns were recorded with a Phylips diffractometer in the Bragg-Brentano geometry using a Ni filtered Cu Kα radiation (λ = 1.54056 Å) and a graphite monochromator in the diffracted beam. The X-ray generator worked at 40 kV and 30 mA; the instrument resolution (divergent and antiscatter slits of 0.5°) was determined using standards free from the effect of reduced crystallite size and lattice defects.

N_2 absorption–desorption isotherms were registered at 77 K using a Quantachrome Nova 2200 Multi-Station High Speed Gas Sorption Analyzer. Samples were outgassed for 3 h at 573 K in the degas station. Adsorbed nitrogen volumes were normalized to the standard temperature and pressure. The specific surface area (S_{BET}) was calculated according to the standard BET method [17] in the relative absorption pressure (P/P_0) range from 0.045 to 0.250. The total pore volume (V_t) was obtained from the nitrogen amount adsorbed in correspondence of P/P_0 equal to 0.99. The cylinder diameter size (w_{BJH}) was calculated by the BJH method [18]. The pore wall thickness (t) was then estimated using the equation:

$$t = a_0 - kw \quad (1)$$

where k is a constant that for hexagonal cylinder and pore wall mass density was obtained by using geometrical consideration equal to 0.95 [19].

^{29}Si Cross Polarization–Magic Angle Spinning Nuclear Magnetic Resonance (^{29}Si $\{^1H\}$ CP–MAS NMR) spectra were obtained at room temperature by means of a Bruker Avance II 400 MHz (9.4 T) spectrometer operating at 79.4 MHz for ^{29}Si nucleus with a MAS rate of 5 kHz, 4096 scans, contact time of 8 ms and repetition delay of 8 s. A contact time of 8 ms was optimized on the samples through variable contact time (VCT) experiments and the optimization of the Hartmann–Hanh condition [20] was obtained by means of a Q8M8 ($Si[(CH_3)_3]_8Si_8O_{20}$) standard. Samples were compressed in 4 mm zirconia rotors with Kel-F (PCTFE) caps.

XPS measurements were performed with an ESCALAB-Mk II (VG Scientific) electron spectrometer. Samples were excited with Mg Kα radiation ($h\nu$ = 1253.6 eV). The total energy resolution of the instrument was 1.2 eV as measured by half width (FWHM) of the Ag $3d_{5/2}$ photoelectron peak. Powdered samples were pressed into 12-mm-diameter stainless-steel sample holders. The glass reactor was opened in a glove box connected to the fast entry lock of the XPS instrument. The sample was transferred to its holder without exposure to air. After introduction into the preparation chamber of the electron spectrometer, the sample was evacuated to 10^{-6} – 10^{-7} Pa, and transferred to the analysis chamber for XPS measurements. The following photoelectrons were recorded: C 1s, O 1s, Si 2p and Mn 2p. Because of a rather low electrical conductivity, sample surface was charged during XPS measurements by +4.5 to +5.5 eV, and therefore, all binding energies were corrected using the C 1s peak centred at 284.6 eV as a reference. In the cases when Ar^+ ion bombardment was applied and the C 1s intensity was very weak, the spectra were referred to the O 1s line at 532.6 eV. The energy of Ar^+ ions was 3 eV with a beam density 12.5 μA cm^{-1} (AG21 ion gun, VG Scientific). Samples were rotated during the ion bombardment to minimize shadowing effects.

The binding energies of C 1s, O 1s, Si 2p and Mn 2p core electron levels were determined by computer fitting the measured spectra and were referenced to the C 1s XPS signal at 284.6 eV. The binding energies are accurate within 0.1 eV. The surface atomic ratios were calculated as the ratio of the corresponding peak intensities, corrected with theoretical sensitivity factors based on Scofield's photoionisation cross-sections in order to obtain information on the structure of the surface and the dispersion of the active phases [21]. The Mn 2p and O 1s lines were decomposed using an iterative least-squares program, the curves being taken as 85% Gaussian and 15% Lorentzian.

Catalytic activity was determinate in the n-hexane oxidation reaction that was carried out in a flow type glass reactor at atmospheric pressure with a catalyst loading of about 0.2 cm^3 (fraction 0.25–0.31 mm). The reaction products were analyzed by a HP 5890 gas chromatograph equipped with a thermal conductivity detector and HP_PLOT/Q capillary column. Helium was used as carrier gas. All gas lines of the apparatus were heated at 80 °C to minimize the n-hexane adsorption on tube walls. Matheson mass flow controllers were used to keep gas flow rates stable. n-Hexane was used both for calibration and oxidation. The gas chromatograph was calibrated against known concentrations of hexane. The conversion was calculated as the ratio of converted to inlet quantity of hexane from the respective peak areas.

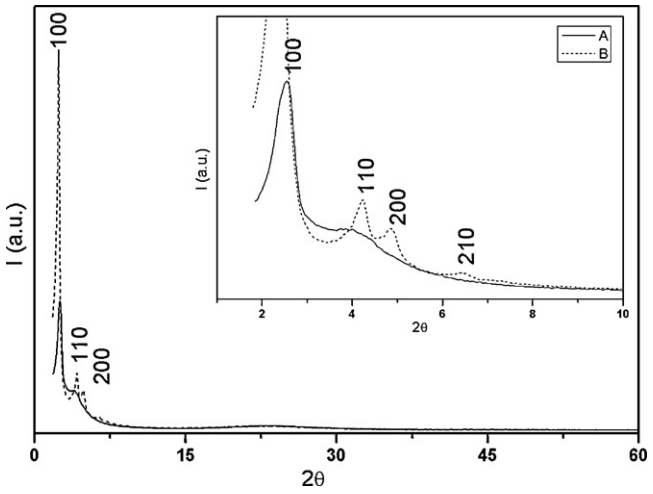

Fig. 1. XRD patterns of A and B samples.

3. Results and discussion

XRD diffraction patterns of MCM-41 materials (sample A and B) are reported in Fig. 1. An enlargement of the XRD pattern is reported in the inset of the figure.

In both samples, the XRD patterns exhibit a high-intensity (1 0 0) and three low-intensity (1 1 0, 2 0 0 and 2 1 0) reflections which are characteristic of the hexagonal structure [22]. The XRD pattern of sample B show well-separated (1 1 0), (2 0 0) and (2 1 0) reflections indicating a better degree of structural ordering than the sample A. This finding is ascribed to the basic pH of the synthesis, in agreement with previous results [23]. XRD diffraction patterns of MCM-41 references (called A' and B') and of Mn-MCM-41 samples with different Mn/Si atomic ratio are reported in Fig. 2. An enlargement of the lower 2θ range XRD pattern is reported in the inset.

All XRD patterns indicate that samples maintain the hexagonal lattice symmetry after the impregnation. The better degree of structural ordering of the sample B has been maintained after the impregnation. The d_{100} spacing, corresponding to the plane distance, was computed using the Bragg's law. The d_{100} spacing, in the hexagonal structure, is correlated with the adjacent pores centre-centre distance, a_0, by means of the following equation [24]:

$$a_0 = \frac{2d_{100}}{\sqrt{3}} \quad (2)$$

The calculated a_0 values for each sample are reported in the Table 1.

The hexagonal unit cell parameter, a, of A, and B samples does not significantly change with the manganese quantity. The small variations are in the experimental errors. This finding shows that

Table 1
Structural data obtained from the XRD pattern analysis of A, B, A', B' and Mn-MCM-41 samples (a_0, lattice parameter; S_{BET}, specific surface area; w_{BJH}, pore width; V_t, total pore volume; t, wall thickness).

Sample	a_0 (Å)	S_{BET} (m^2 g^{-1})*	w_{BJH} (Å)	V_t (cc/g)	t (Å)
A	43(1)	–	–	–	–
A'	42(1)	863	26	0.71	17
Mn/Si 0.012	42(1)	922	24	0.68	20
Mn/Si 0.05	42(1)	1008	15	0.82	27
B	42(1)	–	–	–	–
B'	41(1)	931	24	0.76	18
Mn/Si 0.006	41(1)	979	23	0.78	19
Mn/Si 0.025	41(1)	981	23	0.80	19

* The uncertainty on the S_{BET} values is 5%.

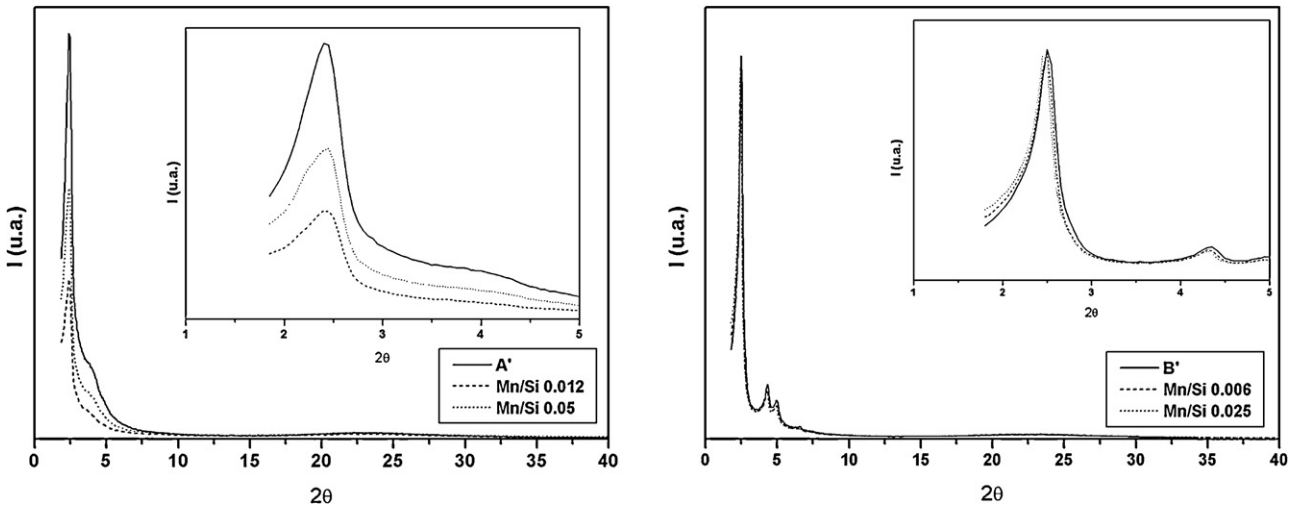

Fig. 2. XRD patterns of A', B' and of Mn-MCM-41 samples.

the nanostructure of the MCM-41 possesses a high thermal stability independently on the pH of the preparation environment, at the used experimental molar ratio, and on the manganese quantity.

No reflections related to the manganese oxide phases were observed in the high angle region of XRD patterns, either at higher manganese content. This suggests the presence of an amorphous and/or very small manganese crystalline species dispersed within silica channels, in agreement with previous studies [25].

The N_2 adsorption–desorption isotherms of A', B' and of the impregnated samples are reported in Fig. 3.

The characteristic type IV-isotherm of MCM-41 [26] does not significantly change with the manganese quantity. Three well-defined regions may be identified: (1) a slow increase in nitrogen uptake at low relative pressure, corresponding to a monolayer-multilayer adsorption on the pore walls; (2) a sharp step at intermediate relative pressures indicative of a capillary condensation within mesopores; (3) a plateau with a slight inclination at high relative pressure associated with multilayer adsorption on the external surface of the materials [26]. The specific surface area (S_{BET}), the total pore volume (V_t), the cylinder diameter size (w) and the pore wall thickness (t) values are reported in Table 1.

The specific surface area S_{BET} values of A' and B' samples are slightly different. A S_{BET} increase with a consequent w_{BJH} pore size decrease and pore wall thickness increase has been observed in the impregnated Mn-MCM-41 prepared starting from the sample A. No significant change of w_{BJH} and of t has been observed in the samples prepared starting from the sample B.

The ^{29}Si $\{^1H\}$ CP–MAS NMR spectra of A', B' and of the impregnated samples are reported in Fig. 4.

Each ^{29}Si $\{^1H\}$ CP–MAS NMR spectrum of Fig. 4 is due to the contribution of three peaks: the first peak, $Q2$, centred at around −90 ppm, is attributed to the geminal silanols, the second peak, $Q3$, at around −100 ppm, is attributed to the silicon atoms bearing one hydroxyl group and the third peak, $Q4$, at around −109 ppm, is attributed to the silicon atoms without hydroxyl groups [27,28].

Since the ^{29}Si $\{^1H\}$ CP–MAS NMR technique is based on the magnetization transfer from ^1H to ^{29}Si nuclei, the peak intensities are related to the total number of protons near the silicon atoms. As a consequence a straight quantification of the different silicon groups is not possible. However, as the bare and the functionalized MCM-41 spectra show the same chemical shifts and the same cross polarization dynamic, the relative intensities of the three different silicon contributions in the three samples are still reliable because

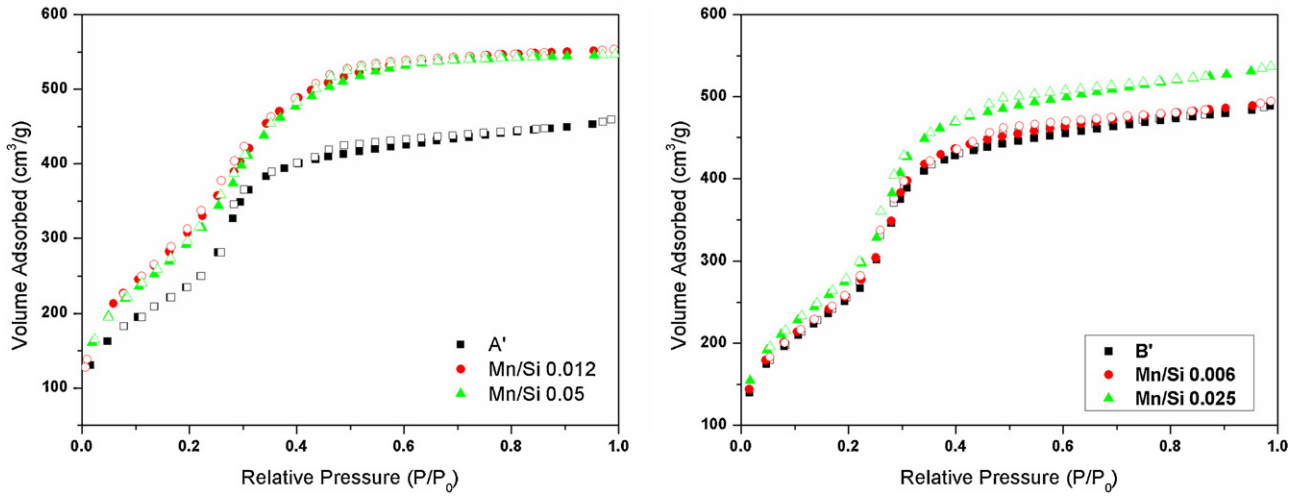

Fig. 3. N_2 adsorption isotherms of A', B' and of Mn-MCM-41 samples.

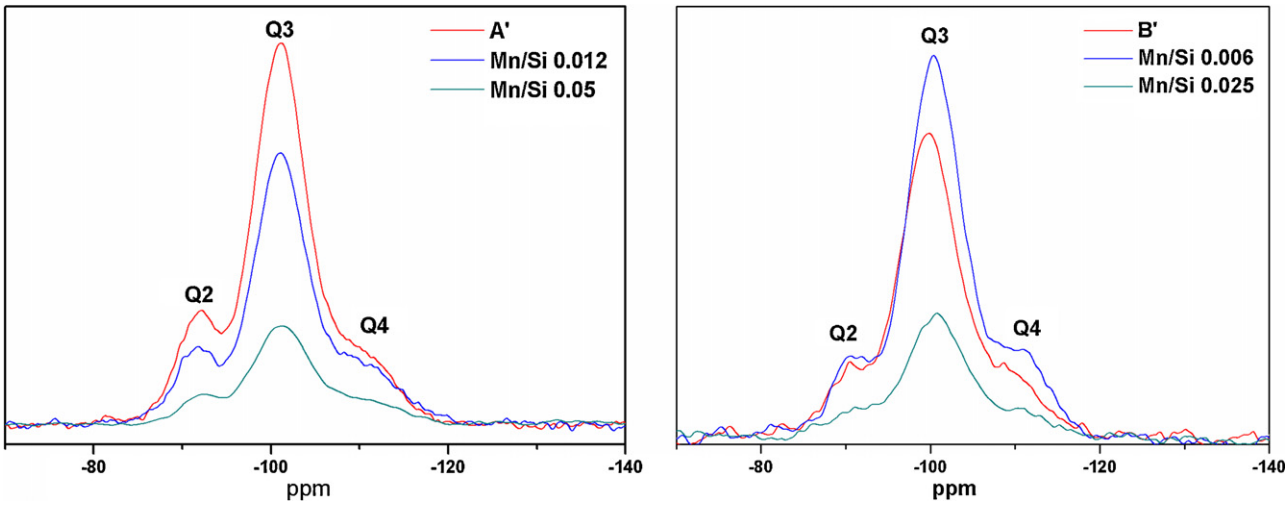

Fig. 4. ^{29}Si {^{1}H} CP–MAS NMR spectra of A', B' and of Mn-MCM-41 samples.

the variation of the contact time does not modify the relative intensity distribution of the signals. Then, the deconvolution of each spectrum has been performed to calculate the single contributions of the three signals.

The relative values of these three NMR signals are reported in Table 2.

The presence of the manganese does not cause any change on the MCM-41 obtained at basic pH, while some modifications have been observed in the MCM-41 prepared at acid pH. In particular, the *Q*4 value increases with the manganese quantity from a relative value of 16.4% for the pure silica to a value of 23.3% for the sample with the highest quantity of manganese. The *Q*2 and *Q*3 bands values decrease from 18.6 to 13.7% and from 65.0 to 59.6%, respectively. This behaviour demonstrates that a modification on the MCM-41 surface occurs when it is functionalized with the manganese, according to previous studies [15]. The *Q*4 increase together with the *Q*2 and *Q*3 decrease indicates that the silicon species bearing the hydroxyl groups strongly interact with the manganese species. The modification in the MCM-41 structure is probably caused by the conversion of the $(Si–O)_3–Si–OH$ groups and of the $(Si–O)_2–Si–(OH)_2$ groups in $(Si–O)_3–Si–O–Mn$ groups.

The surface region of the samples was investigated using XPS to obtain the manganese oxidation state. The BE values obtained for Si 2p (spectra not reported) correspond with literature values for SiO_2 frameworks [29]. The high-resolution XPS spectra in the region of O 1s and of Mn 2p are reported in Fig. 5.

The silica composition presents oxides and hydroxides, hence contributions of species to the O 1s spectrum. The spectrum was fitted by constraining O_2 and OH_2 peaks to different intensities and FWHM values. Two types of oxygen peaks were found in the impregnated samples, one around 532.6 eV, assigned to oxygen in a Si–O–Si framework [30], and the other, a very small contribute, at 529.8 eV, which includes physisorbed hydroxyl groups, and chemisorbed or structurally bound H_2O in contact with the surface.

Table 2
Peak areas obtained by the deconvolution of the ^{29}Si {^{1}H} CP–MAS NMR spectra.

Sample	*Q*2	*Q*3	*Q*4
A'	19	65	16
Mn/Si 0.012	17	59	24
Mn/Si 0.05	14	60	26
B'	13	65	22
Mn/Si 0.006	12	68	20
Mn/Si 0.025	13	65	23

The uncertainty on the *Q* area values is 5%.

Table 3
XPS binding energies of O 1s and Mn $2p_{3/2}$.

Sample	Binding energy (eV)	
	O 1s	Mn $2p_{3/2}$
A'	532.6	–
Mn/Si 0.012	532.5	641.7
Mn/Si 0.05	532.7	641.6
B'	532.5	–
Mn/Si 0.006	532.7	641.3
Mn/Si 0.025	532.5	641.3

The binding energies (BE) of the O 1s and Mn 2p band, obtained calibrating the spectrum using the Si 2p peak at 103.4 eV, are reported in Table 3.

The BE values for Mn 2p are centred at 653 and 641 eV for the $2p_{1/2}$ and $2p_{3/2}$, respectively. Because of the differences in BE values from different reports, identification of the type of manganese oxides present in a mixed-valent system is difficult [31]. The Mn $2p_{3/2}$ value, 641.7 eV, in the Mn-MCM-41 samples obtained starting from acid pH together with the spin orbital splitting ΔE equal to 11.6 eV are in the range of those reported for MnO_2 and of Mn_2O_3 [32]. The Mn $2p_{3/2}$ value, 641.3 eV, in the Mn-MCM-41 samples obtained starting from basic pH together with the spin orbital splitting ΔE equal to 12 eV are in the range of those reported for MnO. According to literature [33,34], the Mn species introducted into a silicate frameworks depend on the pH value.

4. Catalytic activity

The catalytic activity was determinate using the reaction of oxidation of *n*-hexane at different temperature. H_2O and CO_2 were the only detectable reaction products. The percentage of conversion was calculated as the ratio of converted to inlet quantity of hexane. The temperature dependence of the complete *n*-hexane oxidation over the Mn-MMC-41 samples is shown in Fig. 6.

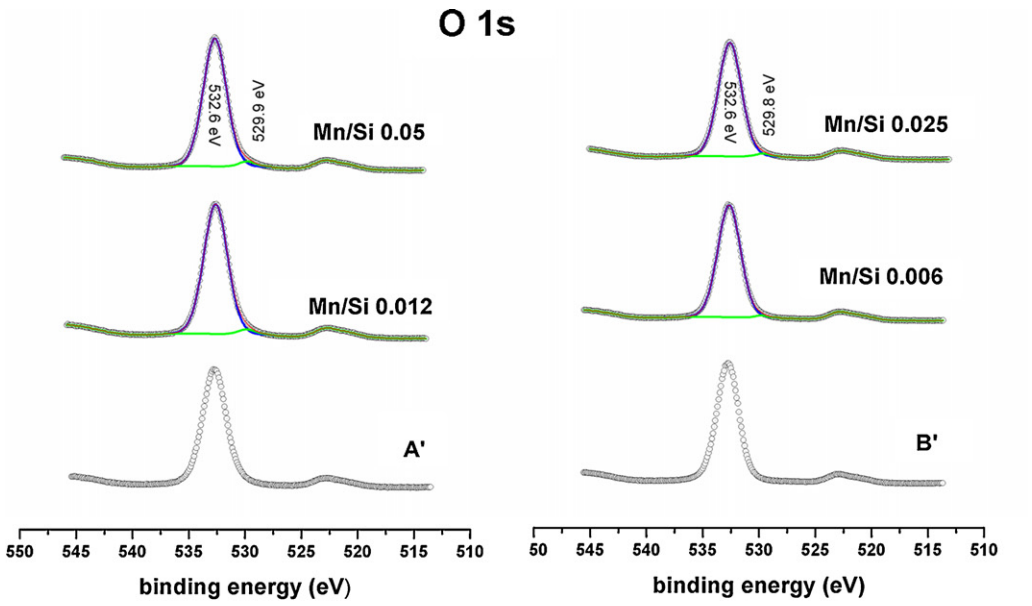

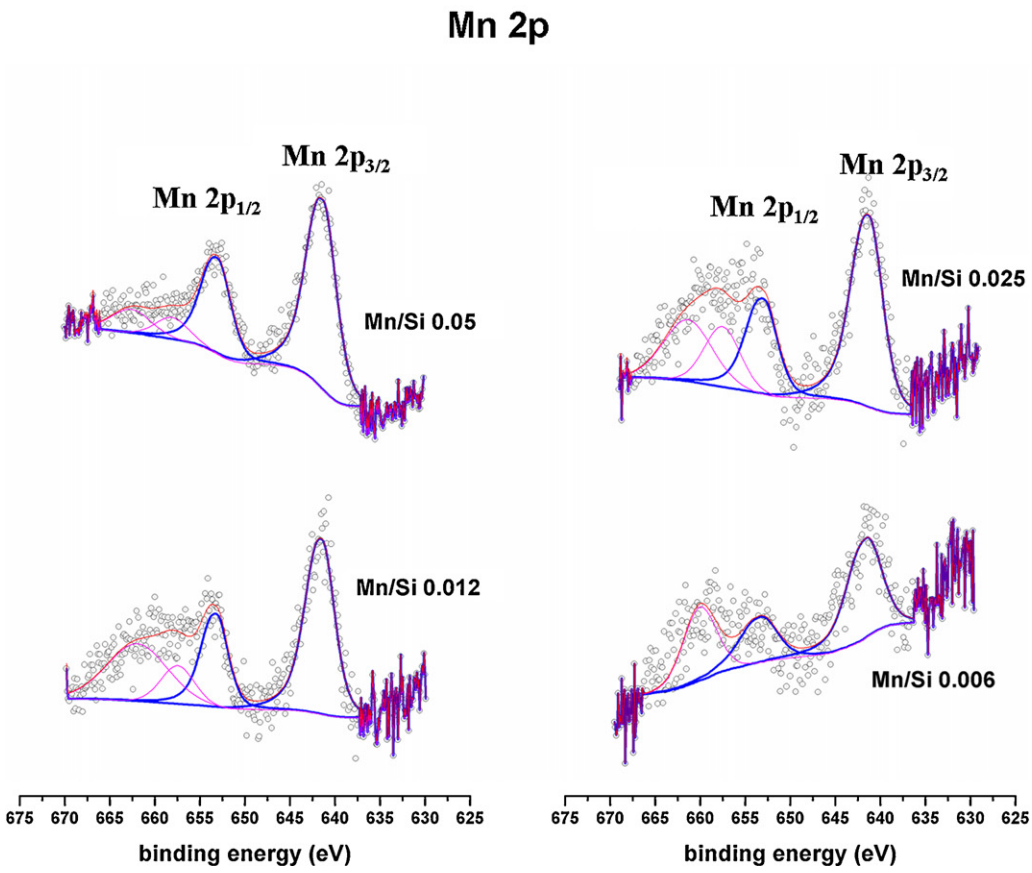

Fig. 5. High-resolution XPS spectra of the samples in the region of O 1s and of Mn 2p.

The temperature dependence of *n*-hexane conversion over Mn-MCM-41 samples having Mn/Si ratio equal to 0.012 and 0.025 showed a similar trend. The catalysts are active at temperature higher than 400 °C. A different behaviour was notice for the Mn-MCM-41 sample having Mn/Si ratio equal to 0.05. The catalyst is active around 300 °C even if the complete oxidation of *n*-hexane occurs around 420 °C. Then, the MnO species in the MCM-41 prepared in basic condition leads to an increase of the catalyst activity in this type of reaction. It is well known that the transient metal oxides operate in complete hydrocarbon oxidation by redox type mechanism, according to which the oxide, after the hydrocarbon oxidation, is regenerated by the oxygen-containing gaseous phase. In this way, the catalytic behaviour can be correlated to the manganese oxides reducibility. This

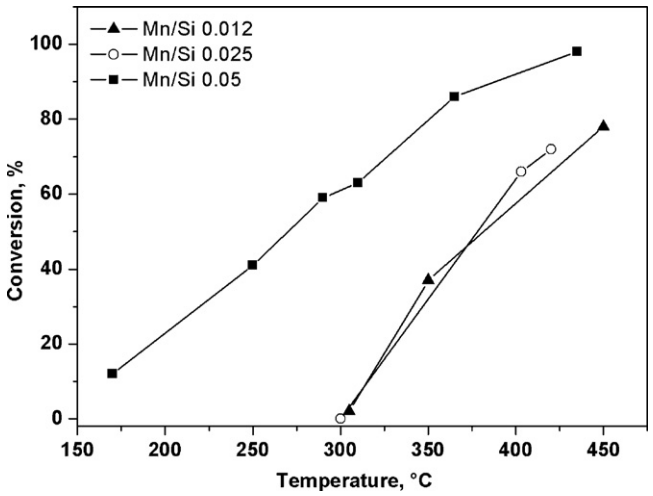

Fig. 6. Temperature dependence of *n*-hexane conversion over Mn-MCM-41 samples.

finding, being low the MnO_x, indicates that a strong interaction with the mesoporous support in the final catalyst occurred [33,34].

5. Conclusions

The incipient wetness method revealed a good method to obtain a composite material constituted by MCM-41 and manganese oxides. The maintenance of the hexagonal structure of MCM-41 after the impregnation was confirmed by XRD data analysis. In all samples the MCM-41 specific surface area does not significantly change with increasing of manganese quantity.

The pH value used for the preparation of the MCM-41 influences some of characteristic of the impregnated samples. In fact, the material obtained at basic pH has a better degree of structural ordering, which is maintained after the impregnation.

On the contrary, the impregnated samples, prepared starting from the material obtained at acid pH, are different. In particular, the pore diameter decreases with the introduction of manganese within the pores of silica surface together with a $Si–(Si–O)_4$ groups increase and an $(Si–O)_3–Si–OH$ groups reduction, observed by nitrogen porosimetry and $^{29}Si\ \{^1H\}$ CP–MAS NMR measurements, respectively.

The XPS spectra showed that, depending on the pH of supports preparation, different manganese oxide species are formed (MnO, MnO_2 and of Mn_2O_3), which determinate a different catalytic activity. Finally, catalytic test indicated that the Mn-MCM-41 materials can be used in the oxidation reaction of hydrocarbons. From the given tests, it has been clearly seen that the efficiency of this type of catalytic system increases with the temperature and with manganese quantity.

Acknowledgements

The authors would like to thank the MIUR for supporting this research through the PRIN 2007 prot. 20077R3PXF_002 “New nanocomposites preparation for optical, electric and magnetic applications”. NMR experimental data have been provided by Centro Grandi Apparecchiature – UniNetLab – Università di Palermo funded by P.O.R. Sicilia 2000–2006, Misura 3.15 Azione C Quota Regionale.

References

[1] I. Arends, R.A. Sheldon, M. Wallau, U. Schuchardt, Angew. Chem. Int. Ed. Engl. 36 (11) (1997) 1144.
[2] H. Yokoyama, Science 256 (1992) 66.
[3] P. Oliveira, et al., Catal. Lett. 114 (2007) 192–197.
[4] A. Sayari, Chem. Mater. 8 (1996) 1840.
[5] A. Corma, Chem. Rev. 97 (1997) 2373.
[6] S. Biz, M.I. Occelli, Catal. Rev. 40 (1998) 329.
[7] J.Y. Ying, C.P. Mehnert, M.S. Wong, Angew. Chem. Int. Ed. 38 (1999) 56.
[8] S. Vetrivel, A. Pandurangan, J. Mol. Catal. A: Chem. 246 (2006) 223–230.
[9] D. Zhao, D. Goldfarb, J. Chem. Soc., Chem. Commun. (1995) 875.
[10] A. Ramanathan, T. Archipov, R. Maheswari, U. Hanefeld, E. Roduner, R. Glдser, J. Phys. Chem. C 112 (2008) 7468–7476.
[11] J. Xu, Z. Luan, T. Wasowicz, L. Kevan, Microporous Mesoporous Mater. 22 (1998) 179.
[12] K.M. Parida, S.S. Dash, S. Singha, Appl. Catal. A: Gen. 351 (2008) 59–67.
[13] P. Oliveira, A. Machado, A.M. Ramos, I.M. Fonseca, F.M. Braz Fernandes, A.M. Botelho do Rego, J. Vital, Catal. Lett. 114 (2007).
[14] S. Vetrivel, A. Pandurangan, J. Mol. Catal. A: Chem. 227 (2005) 269–278.
[15] M.L. Saladino, A. Spinella, E. Caponetti, A. Minoja, Microporous Mesoporous Mater. 113 (2008) 490–498.
[16] J. Santamaria-Gonzales, J. Merida-Robles, M. Alcantara-Rodrıguez, P. Maireles-Torres, E. Rodrıguez-Castellon, A. Jimenez-Lopez, Catal. Lett. 64 (2000) 209.
[17] S. Brunauer, P.H. Emmett, E. Teller, J. Am. Chem. Soc. 60 (1938) 309.
[18] M. Kruk, V. Antchshuk, M. Jaroniec, A. Sayari, J. Phys. Chem. B 103 (103) (1999) 10670.
[19] M. Kruk, M. Jaroniec, Y. Sakamoto, O. Terasaki, R. Ryoo, C.H. Ko, J. Phys. Chem. B 104 (2000) 292.
[20] S.R. Hartmann, E.L. Hahn, Phys. Rev. 128 (1962) 2042.
[21] H.J. Scofield, J. Electron Spectrosc. Relat. Phenom. 8 (1976) 129.
[22] G. Behrens, G.D. Stucky, Angew. Chem., Int. Ed. Engl. 32 (1993) 696, and references therein.
[23] J. Zhang, D. Goldfarb, J. Mesoporous Microporous Mater. 48 (2001) 143–149.
[24] J. Aguado, D.P. Serrano, J.M. Escola, Microporous Mesoporous Mater. 34 (2000) 43.
[25] Q. Zhang, Y. Wang, S. Itsuki, T. Shishido, K. Takehira, J. Mol. Catal. A: Chem. 188 (2002) 189–200.
[26] S.J. Gregg, K.S.W. Sing, Adsorption, Surface Area and Porosity, 2nd ed., Academic Press, London, 1982.
[27] M. Luhmer, J.B. Espinose, H. Hommel, A.P. Legrand, Magn. Reson. Imaging 14 (1996) 911.
[28] A.Y. Stakheev, E.S. Shpiro, J. Apijok, J. Phys. Chem. 97 (1993) 5668.
[29] I. Bertoti, G. Varsanyi, G. Mink, T. Szekely, J. Vaivads, T. Millers, J. Grabis, Surf. Interface Anal. 12 (1998) 527.
[30] D. Das, G. Ravichandran, D.K. Chakrabarty, Appl. Catal. A-Gen. 131 (1995) 335–345.
[31] R. Dula, R. Janik, T. Machej, J. Stoch, R. Grabowski, E.M. Serwicka, Catal. Today 119 (2007) 327–331.
[32] J.F. Moulder, W.F. Sticke, P.E. Sobol, K.D. Bombel, in: J. Castain, Minnesota (Eds.), Handbook of X-ray Photoelectron Spectroscopy, Second ed., Perkin-Elmer Corporation, Physical Electron Division, USA, 1992.
[33] N.N. Tusar, S. Jank, R. Glser, ChemCatChem 3 (2011) 254–269.
[34] A. Ramanathan, T. Archipov, R. Maheswari, U. Hanefeld, E. Roduner, R. Glser, J. Phys. Chem. C 112 (2008) 7468–7476.